Performance Evaluation of Massive MIMO with Beamforming and Non Orthogonal Multiple Access based on Practical Channel Measurements

Eric Pierre Simon, Joumana Farah, Pierre Laly

Performance Evaluation of Massive MIMO with Beamforming and Non Orthogonal Multiple Access based on Practical Channel Measurements

Eric Pierre Simon[1], Joumana Farah[2], Pierre Laly[1]

***Abstract*—This paper presents a comprehensive performance analysis of a massive multiple-input multiple-output (MIMO) system using non-orthogonal multiple access (NOMA) in both indoor and outdoor environments, based on practical channel measurements. The latter are performed using frequency-domain channel sounding experiments conducted at 3.5 GHz with 18 MHz bandwidth. Multi-user beamforming and NOMA clustering are used in the massive MIMO system. The system performance is evaluated in terms of sum-rate capacity for two precoding schemes: zero-forcing (ZF) and maximum ratio transmission (MRT). Two inter-beam power allocation (PA) schemes are investigated: equal PA and water filling. Fractional transmit PA (FTPA) is used to perform intra-cluster PA between paired users. The study allows the identification of practical scenarios that are propitious to NOMA with beamforming. Results show that NOMA is particularly interesting with MRT, compared to ZF, especially when combined with water filling. However, ZF generally outperforms MRT for all system configurations.**

***Index Terms*—Massive MIMO, NOMA, Zero-Forcing Beamforming, Maximum Ratio Transmission Beamforming, Power Allocation, Channel sounding.**

I. Introduction

With the advent of 5G communications, Non Orthogonal Multiple Access (NOMA) has recently spurred a large amount of research work in a broad range of applications [1]. By a judicious power multiplexing, NOMA greatly outstrips the performance of its predecessor OMA (Orthogonal Multiple Access), widely used in 4G systems. It has also proved to be an important ally of multi-antenna transceivers in leveraging both energy and spectral efficiency of wireless systems, either in collocated [2] [3] or distributed antenna configurations [4]. Power-domain NOMA allows multiplexing two or several users on the same frequency subband by taking advantage of their channel gain difference [5]. At the receiver, user separation is done using successive interference cancellation (SIC). The use of NOMA in MIMO systems with zero-forcing (ZF) beamforming (BF) is explored in [6] where clustering and PA are done so as to minimize inter-cluster and inter-user interference. In [2], joint optimization of BF and power allocation (PA) is considered for both best-effort and rate-constrained users, with random user pairing. [7] considers a two-user single-beam MIMO system with intra-beam PA for sum-rate maximization. In [8], a ZF BF technique is proposed for downlink MIMO-NOMA, with dynamic PA and user-clustering so as to mitigate inter-cluster interference. [2] [6] [7] [8] show the important gain obtained with NOMA vs. OMA in the MIMO-BF context; nevertheless, these works are based on simulated transmission environments. It is not straightforward to validate their results in practical scenarios; more specifically, the design of user clustering and BF in indoor and outdoor is essential to confirm the viability of NOMA with massive MIMO in realistic environments. In [9], the results of channel measurement campaigns for massive MIMO with OMA are analyzed to validate three theoretical characteristics of massive MIMO systems: channel hardening, user orthogonality, and spatial covariance matrix rank. In [10], experimental measurements of user throughput are conducted in outdoor, for NOMA with open-loop 2x2 or 4x2 MIMO, to validate the system-level performance of MIMO-NOMA for two or three users in the system. To the best of our knowledge, no previous work has tackled the validation of NOMA clustering and BF in massive antenna transmission through practical channel sounding techniques. This paper aims at studying the viability of NOMA when combined with massive MIMO, by drawing important conclusions on the user positions propitious for clustering, depending on the environment and the PA and BF techniques. To this aim, this letter is organized as follows: In section II, we start by describing the experimental setup used in our channel measurement campaign. Then, section III is dedicated to the system model adopted for the integration of channel measurements. Section IV describes the NOMA clustering and PA techniques used in our system. Throughput analysis is conducted in section V for different transmission scenarios and environments.

II. Channel measurements

In this section, we present the measurement campaigns performed on massive MIMO channels, on which we base our study to assess the system performance with different BF and PA strategies. We start by introducing the measurement equipment. Then, we describe the outdoor and indoor environments where measurements are carried out.

A. Measurement setup

Narrowband frequency-domain channel sounding measurements [11] are performed in indoor and outdoor. A vector network analyzer (VNA) of type Agilent Technologies E5071C

E.P. Simon and P. Laly are with the University of Lille and IEMN lab, Villeneuve d'Ascq, France. E.P. Simon is also a member of IRCICA. e-mail: eric.simon@univ-lille.fr.

J. Farah is with the Department of Electricity and Electronics, Faculty of Engineering, Lebanese University, Roumieh, Lebanon. e-mail: joumana-farah@ul.edu.lb.

is used to probe the radio channel in an 18 MHz bandwidth centered at 3.5 GHz. In this frequency band, 1200 uniformly spaced frequency points (subcarriers) are sampled with a frequency spacing of 15 KHz, corresponding to the LTE/LTE Advanced mobile system parameters [12]. The feeder cables for the transmitting and receiving antennas are MegaPhase high performance RF coaxial cables. They are included in the VNA calibration so that their effect is canceled in the channel measurement. At the transmitter, a virtual 2-D patch antenna array is created by an automated displacement system driven by a stepper motor. The virtual array is a vertical uniform rectangular array (URA), where measurements are performed over a 10×10 rectangular grid with 0.5λ spacing along X and Y, λ being the wavelength at 3.5 GHz. For each antenna position, the VNA acquires 10 successive realizations of the whole frequency range, which are then averaged for the reduction of measurement noise. The receiver is equipped with a single fixed antenna. This antenna is the EM-6116 omnidirectional antenna in our outdoor measurements, whereas a patch antenna is used for indoor. In indoor, both transmit and receiver antennas are positioned at 1.50m above ground level. In outdoor, the transmitter is positioned at a height of approximately 10m in order to imitate a cellular configuration with a base station. Fig. 1 shows the transmitter (Tx) and receiver (Rx) in the outdoor environment. Note that the measurement campaign is carried out outside the regular working hours, because channel sounding with virtual antenna arrays requires a static radio channel without motion. The set of measurements is constituted by fixing the Tx position while moving Rx at different positions.

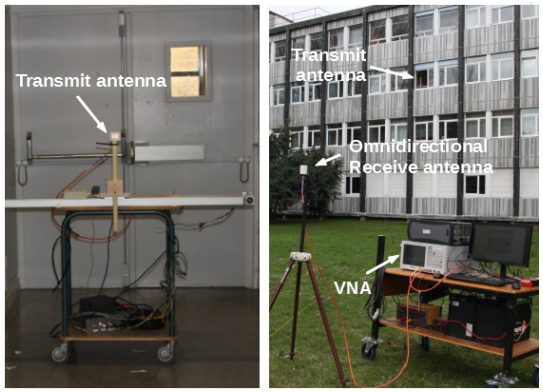

Fig. 1: Practical setup for channel measurements

B. Measurement Environments

The outdoor environment considered in this study is a semi-urban area located at the campus of the university of Lille, France. Fig. 2 presents the measurement environment with the Tx (in red) and Rx antenna locations. A total of 8 Tx-Rx links is measured in outdoor, corresponding to Rx i ($i = 1, \cdots, 8$) in Fig. 2 left. The indoor environment is the first floor of a typical office building on the campus. Two rows of rooms are situated on both sides of a 40m long corridor. The office rooms are separated by plaster walls. A map of this scenario is shown

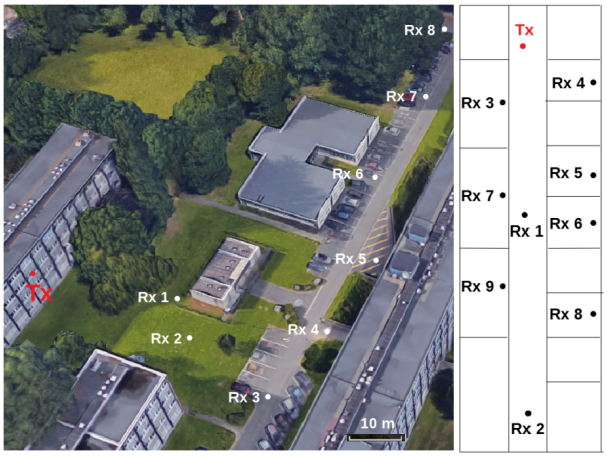

Fig. 2: Outdoor (left) and indoor (right) environments with Tx and Rx locations

in Fig. 2 right, with the positions of the Tx and 9 different receivers Rx i ($i = 1, \cdots, 9$).

III. System Model

Consider a downlink massive MIMO system with K users. The Tx plays the role of a base station (BS) equipped with $M = 100$ antennas, while each position of the Rx corresponds to a different user equipped with a single antenna. The BS performs BF with N beams ($N \leq K \leq M$). The grouping of multiple users within the same beam using NOMA is defined as a cluster. In this study, the maximum number of users per cluster is two. Let $\mathbf{h}_{n,1}$ and $\mathbf{h}_{n,2}$ denote their $1 \times M$ channel vectors. In each cluster, the user having the higher (resp. lower) channel gain $\|\mathbf{h}_{n,1}\|$ (resp. $\|\mathbf{h}_{n,2}\|$) is defined as the strong (resp. weak) user, and is referred to by index 1 (resp. 2). The number of clusters is $C \leq N$, i.e., some of the beams support single users. Hereafter, we describe the transceiver system for a given frequency subband. Nevertheless, for the sake of notation concision, the subband index is dropped in the following expressions. Let x_n be the signal transmitted on beam n with power P_n. The signal transmitted by the multi-antenna system is an $M \times 1$ vector defined as follows:

$$\mathbf{x} = \sum_{n=1}^{N} \sqrt{P_n} \mathbf{w}_n x_n, \tag{1}$$

where $\mathbf{w}_n$ is the n^{th} row of the $M \times N$ precoding matrix $\mathbf{W}$. In a two-user beam, x_n is decomposed as $x_n = \sqrt{\alpha_{n,1}} s_{n,1} + \sqrt{\alpha_{n,2}} s_{n,2}$, where $s_{n,1}$ and $s_{n,2}$ are the transmitted signals of the strong and weak users respectively, with $\alpha_{n,1} + \alpha_{n,2} = 1$. Without loss of generality, the first C beams are clusters, while the subsequent ones are single-user beams. $E[|s_{n,i}|^2] = 1$, $n = 1, \cdots, C$, $i = 1, 2$, and $E[|x_n|^2] = 1$, $n = 1, \cdots, N$. The received signals for the users belonging to clusters are:

$$y_{n,i} = \mathbf{h}_{n,i}\mathbf{x} + n_{n,i}, i = 1, 2 \text{ and } n = 1, \cdots, C, \tag{2}$$

where $y_{n,1}$ and $y_{n,2}$ are the received signals for the strong and the weak users, respectively. $n_{n,i}$ is an i.i.d. additive

white complex Gaussian noise (AWGN) with zero mean and variance σ_n^2. For single-user beams:

$$y_n = \mathbf{h}_n \mathbf{x} + n_n, n = C+1, \cdots N. \quad (3)$$

Similarly to [6], BF is performed based on the channel gains of the strong users in clusters. An $N \times M$ channel matrix $\mathbf{H}$ is constituted by the channel vectors of the strong users within clusters and unique users of single-user beams:

$$\mathbf{H} = \left[\mathbf{h}_{1,1}^T, \cdots, \mathbf{h}_{C,1}^T, \mathbf{h}_{C+1}^T, \cdots, \mathbf{h}_N^T\right]^T. \quad (4)$$

For ZF BF, precoding is done using $\tilde{\mathbf{W}} = \mathbf{H}^H(\mathbf{H}\mathbf{H}^H)^{-1}$, while for MRT $\tilde{\mathbf{W}} = \mathbf{H}^H$. Then, the beams precoding vectors are obtained by normalizing each column of $\tilde{\mathbf{W}}$, i.e. $\mathbf{w}_n = \frac{\tilde{\mathbf{w}}_n}{\|\tilde{\mathbf{w}}_n\|}$, where $\tilde{\mathbf{w}}_n$ is the n^{th} column of $\tilde{\mathbf{W}}$.

The received signal of the strong user in a cluster can be decomposed as:

$$y_{n,1} = g_{n,1,n}\sqrt{P_n \alpha_{n,1}} s_{n,1} + g_{n,1,n}\sqrt{P_n \alpha_{n,2}} s_{n,2} + \sum_{k=1, k\neq n}^{N} g_{n,1,k}\sqrt{P_k} x_k + n_{n,1}, \; n = 1, \cdots, C \quad (5)$$

where the equivalent channel gains are given by $g_{n,1,k} = \mathbf{h}_{n,1}\mathbf{w}_k$. The first three terms in (5) correspond respectively to the useful signal, intra-cluster interference (ICI) and inter-beam interference (IBI). As in classical single-input single-output (SISO) NOMA, the strong user can remove ICI by SIC. In the case of ZF BF, IBI can be canceled since $g_{n,1,k} = 0$ for $k \neq n$. The received signal of a weak user is similar to (5). However, ICI is not canceled at the level of weak users. Assuming perfect SIC, the received SINRs are:

$$\text{SINR}_{n,1} = \frac{|g_{n,1,n}|^2 P_n \alpha_{n,1}}{\sum_{k=1,k\neq n}^{N} |g_{n,1,k}|^2 P_k + \sigma_n^2} \quad (6)$$

$$\text{SINR}_{n,2} = \frac{|g_{n,2,n}|^2 P_n \alpha_{n,2}}{|g_{n,2,n}|^2 P_n \alpha_{n,1} + \sum_{k=1,k\neq n}^{N} |g_{n,2,k}|^2 P_k + \sigma_n^2} \quad (7)$$

For a user in beam $n = C+1, \ldots, N$, $g_{n,k} = \mathbf{h}_n \mathbf{w}_k$:

$$\text{SINR}_n = \frac{|g_{n,n}|^2 P_n}{\sum_{k=1,k\neq n}^{N} |g_{n,k}|^2 P_k + \sigma_n^2}. \quad (8)$$

IV. Clustering Technique and Power Allocation

The NOMA clustering technique used in this work is inspired from [6], where a correlation threshold ρ is used. However, unlike [6] which considers a fixed number of clusters regardless of the number of active users in the system, here all users are served simultaneously on all subbands. More specifically, our clustering algorithm starts by identifying the set of user pairs that present a channel correlation exceeding ρ. From this set, the user pair that presents the highest channel difference (estimated by $\|\mathbf{h}_{n,1}\| - \|\mathbf{h}_{n,2}\|$) is selected to constitute the first beam. These users are then removed from the user set. The search is iterated until no more user pair has a correlation higher than ρ. The remaining users are then allocated to separate beams.

As for PA, it is performed in two steps. First, inter-beam PA is realized to determine P_n, $n = 1, \ldots, N$. Two different schemes are studied in this context: equal power and water-filling inter-beam PA. Inspired from the work in [13], where water-filling is used for inter-subband allocation in SISO NOMA, in this work, P_n, $n = 1, \ldots, C$, is determined by the channel gain of the strong user in cluster n. Then, in a second step, intra-beam PA is performed, where $\alpha_{n,i}$, $i = 1, 2$, are determined using Fractional Transmit Power Allocation (FTPA) [5].

V. Performance Evaluation and Conclusion

In this section, we assess the performance of the studied massive MIMO NOMA system with our channel measurements, under different PA and BF strategies. 12 frequency subbands of 100 subcarriers are considered. BF and PA are performed separately on each subband, and the obtained spectral efficiency (calculated using Shannon capacity, based on the estimated SINRs) is averaged over all subbands. As our main goal is to assess the practical performance of NOMA in massive MIMO, each studied user set configuration is taken such that at least one NOMA pair can be formed among the considered users, i.e., at least one user pair fulfills the clustering requirements. For the outdoor scenario, two user sets are defined: $\mathcal{O}_1$ = {Rx 1, Rx 2, Rx 4, Rx 8} and $\mathcal{O}_2$ = {Rx $i, i = 1, \ldots, 8$}. For indoor, we consider: $\mathcal{I}_1$ = {Rx 1, Rx 2, Rx 3, Rx 7}, $\mathcal{I}_2$ = {Rx 5, Rx 6, Rx 7, Rx 9}, and $\mathcal{I}_3$ = {Rx 1, Rx 2, Rx 3, Rx 5, Rx 7, Rx 8}.

Fig. 3 shows the channel correlation of some user pairs examples as a function of the subcarrier index. The pairs selected for NOMA clustering are those presenting a correlation greater than the threshold ρ, fixed at 0.7 in this work: Rx2-Rx4 in outdoor, Rx1-Rx2 and Rx5-Rx6 in indoor, for most of the subbands. Indeed, as the correlation is subband dependent, user grouping can vary from a subband to another. As can be seen in Fig. 2, both outdoor Rx2-Rx4 and indoor Rx1-Rx2 NOMA pairs correspond to users sharing the same line of sight (Los), whereas the Rx5-Rx6 pair corresponds to users in two adjacent rooms, only separated by a plaster wall. This shows that, in addition to LoS users, NOMA clustering can be efficiently applied to users in different indoor conditions.

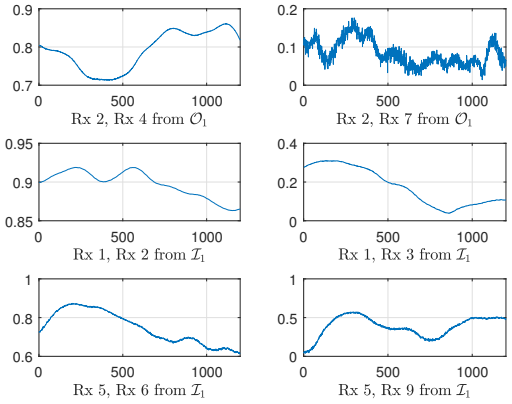

Fig. 3: Channel correlation for different user pairs as a function of the subcarrier index

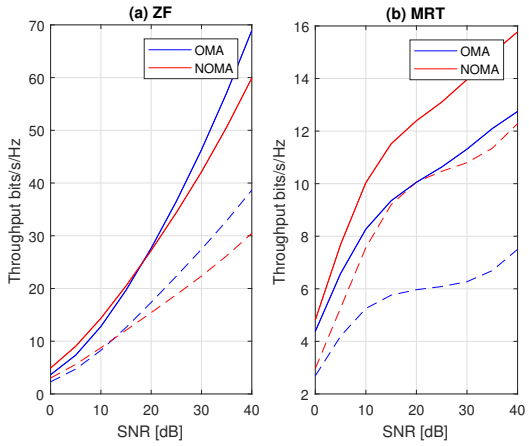

Fig. 4: Outdoor, EP, dashed lines: $\mathcal{O}_1$, continuous lines: $\mathcal{O}_2$

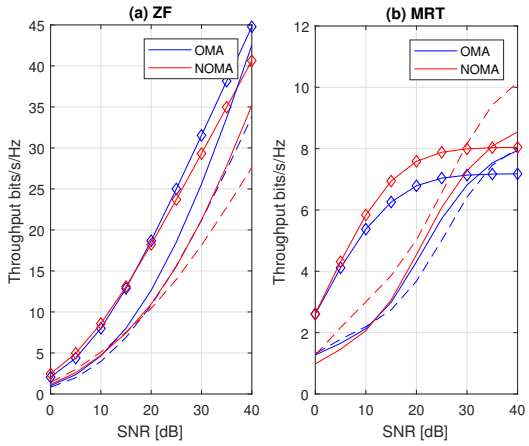

Fig. 5: Indoor, EP, dashed lines: $\mathcal{I}_1$, lines with diamonds: $\mathcal{I}_2$, continuous lines: $\mathcal{I}_3$

Fig. 4 and Fig. 5 show the average throughput obtained for outdoor and indoor user sets respectively, for ZF and MRT BF, and equal power (EP) PA. The performance of OMA is also shown for comparison, where all beams are constituted by single users. The same behaviour is observed in both environments. Regarding MRT, NOMA outperforms OMA for the whole receive SNR (Signal to Noise Ratio) range and all user sets. This is due to the fact that NOMA groups users having strongly correlated channels. It is known that MRT performs well when users in different beams present a low correlation, and its performance quickly degrades when user correlation increases, due to inter-beam interference [14]. Therefore, by grouping the most correlated users within the same beam, NOMA is highly favorable to MRT.

When it comes to ZF, NOMA performs similarly or slightly better than OMA at low SNR, while OMA outperforms NOMA at high SNR. When NOMA is employed with ZF, two contradictory phenomena occur. On the one hand, the grouping of users reduces the number of beams compared to OMA. Recall that for ZF, $\mathbf{h}_n\mathbf{w}_n = \frac{1}{\|\tilde{\mathbf{w}}_n\|}$. Due to Cauchy-Schwartz inequality [15], the fewer rows of $\mathbf{H}$ that a particular $\tilde{\mathbf{w}}_n$ is constrained to be orthogonal to, the smaller its norm, and thus the larger the equivalent channel gains $g_{n,n}$, which is favorable for throughput performance. On the other hand, when NOMA clustering is applied, the weak user suffers from IBI and ICI, which degrades its performance compared to the case where this user occupies a single-user beam. At low SNR, the ICI and IBI powers are negligible with respect to the additive noise variance. Thus, the first phenomenon dominates. However, when the SNR increases, the ICI and IBI are no longer negligible and the second phenomenon dominates, resulting in a poor throughput for the weak user. To illustrate this, we report in Table I the throughput of each user in the set $\mathcal{O}_1$ at SNR=10 and 40 dB, for the first subband. The loss of the weak user Rx 4 penalizes the performance of NOMA at SNR=40 dB compared to OMA.

		Rx1	Rx2	Rx4	Rx8
SNR=10 dB	OMA	4.6	2.8	1.7	0.02
	NOMA	5.1	3.6	0.7	0.03
SNR=40 dB	OMA	14.5	12.5	11.1	1.6
	NOMA	15	13.4	0.9	1.9

TABLE I: Throughput of EP in bits/s/Hz for users in $\mathcal{O}_1$.

		ZF		MRT	
		OMA	NOMA	OMA	NOMA
$\mathcal{O}_1$	SNR=10 dB	9.3-8.2	10-8.7	5.6-5.2	8.8-7.5
	SNR=30 dB	28.6-27.4	23.2-22.3	6.1-6.2	11.8-10.8
$\mathcal{I}_1$	SNR=10 dB	5.4-3.9	6.9-5.1	2.2-2.1	6.9-3
	SNR=30 dB	21.3-21.2	18.2-18.1	6.3-6.4	8.4-8.1

TABLE II: Throughput of WF vs. EP in bits/s/Hz, for $\mathcal{O}_1$ and $\mathcal{I}_1$.

Globally, MRT is significantly outperformed by ZF for all SNR values, in both indoor and outdoor environments. This is due to the fact that MRT aims at maximizing the receive SNR while ZF aims at annihilating the correlation between beams. However, ZF necessitates a pseudo inverse of the channel matrix $(\mathbf{H}^H(\mathbf{H}\mathbf{H}^H)^{-1})$ which has a complexity by the order of O(M^3). Therefore, an efficient implementation of ZF on transmitters with low resources and computational capacities may be unfeasible. When MRT is used in low-complexity transmitters, our study shows that NOMA can significantly increase the system performance.

When using water filling (WF) instead of EP, it is known that subbands having inverse channel gains above the water line are not allocated any power. Therefore, the number of useful beams varies with the SNR and it is inconvenient to show throughput curves in terms of SNR. Instead, some throughput values are reported in Table II. It is clear that the gain obtained with WF towards EP is particularly significant with NOMA for a low SNR.

In conclusion, several beamforming and power allocation scenarios are studied in this letter for a massive MIMO system, under practical channel measurements. The study shows that NOMA with ZF is especially interesting in low SNR regimes. In MRT, NOMA allows an important performance gain in all SNR regions, by judiciously clustering highly correlated users. However, MRT is significantly outperformed by ZF BF for all SNR values, in both indoor and outdoor environments. These conclusions are validated in both outdoor and indoor environments.

REFERENCES

[1] Y. Liu, Z. Qin, M. Elkashlan, Z. Ding, A. Nallanathan, and L. Hanzo, "Non orthogonal multiple access for 5G and beyond," *Proceedings of the IEEE*, vol. 105, no. 12, pp. 2347–2381, 2017.

[2] X. Sun, C. Shen, Y. Xu, S. M. Al-Basit, Z. Ding, N. Yang, and Z. Zhong, "Joint beamforming and power allocation design in downlink non-orthogonal multiple access systems," in *Globecom Workshops (GC Wkshps), 2016 IEEE*. IEEE, 2016, pp. 1–6.

[3] M.-J. Youssef, J. Farah, C. A. Nour, and C. Douillard, "Waterfilling-based resource allocation techniques in downlink non-orthogonal multiple access (NOMA) with single-user MIMO," in *Computers and Communications (ISCC), 2017 IEEE Symposium on*. IEEE, 2017, pp. 499–506.

[4] J. Farah, A. Kilzi, C. A. Nour, and C. Douillard, "Power minimization in distributed antenna systems using non-orthogonal multiple access and mutual successive interference cancellation," *IEEE Transactions on Vehicular Technology*, vol. 67, no. 12, pp. 11 873–11 885, 2018.

[5] A. Benjebbour, A. Li, Y. Saito, Y. Kishiyama, A. Harada, and T. Nakamura, "System-level performance of downlink NOMA for future LTE enhancements," in *Globecom Workshops (GC Wkshps)*. IEEE, 2013, pp. 66–70.

[6] B. Kim, S. Lim, H. Kim, S. Suh, J. Kwun, S. Choi, C. Lee, S. Lee, and D. Hong, "Non-orthogonal multiple access in a downlink multiuser beamforming system," in *Military Communications Conference, MILCOM*. IEEE, 2013, pp. 1278–1283.

[7] Z. Xiao, L. Zhu, J. Choi, P. Xia, and X.-G. Xia, "Joint power allocation and beamforming for non-orthogonal multiple access (NOMA) in 5G millimeter-wave communications," *IEEE Transactions on Wireless Communications*, vol. 17, no. 5, pp. 2961–2974, 2018.

[8] S. Ali, E. Hossain, and D. I. Kim, "Non-orthogonal multiple access (NOMA) for downlink multiuser MIMO systems: User clustering, beamforming, and power allocation," *IEEE Access*, vol. 5, pp. 565–577, 2017.

[9] À. O. Mart´inez, J. O. Nielsen, E. De Carvalho, and P. Popovski, "An experimental study of massive MIMO properties in 5G scenarios," *IEEE Transactions on Antennas and Propagation*, vol. 66, no. 12, pp. 7206–7215, 2018.

[10] A. Benjebbour and Y. Kishiyama, "Combination of NOMA and MIMO: concept and experimental trials," in *2018 25th International Conference on Telecommunications (ICT)*. IEEE, 2018, pp. 433–438.

[11] C. Sanchis-Borras, J.-M. Molina-Garcia-Pardo, M. Lienard, and P. Degauque, "Performance evaluation of MIMO-OFDM in tunnels," *IEEE Antennas Wireless Propag. Lett.*, vol. 11, pp. 301–304, 2012.

[12] "Physical Layer Aspects for Evolved UTRA, TR25-814 (V7.1.0)," 3GPP, Tech. Rep., 2006.

[13] M.-R. Hojeij, J. Farah, C. A. Nour, and C. Douillard, "Resource allocation in downlink non-orthogonal multiple access (NOMA) for future radio access," in *Vehicular Technology Conference (VTC Spring), IEEE 81st*. IEEE, 2015, pp. 1–6.

[14] E. G. Larsson, O. Edfors, F. Tufvesson, and T. L. Marzetta, "Massive MIMO for next generation wireless systems," *IEEE communications magazine*, vol. 52, no. 2, pp. 186–195, 2014.

[15] P. W. Wolniansky, G. J. Foschini, G. Golden, and R. A. Valenzuela, "V-BLAST: An architecture for realizing very high data rates over the rich-scattering wireless channel," in *Signals, Systems, and Electronics*, 1998.